TRI-PP-93-90
Nov 1993

A Method for Correcting the Depth-of-interaction Blurring in PET Cameras

Joel G. Rogers
TRIUMF, 4004 Wesbrook Mall, Vancouver, Canada V6T-2A3

Abstract

A method is presented for the purpose of correcting PET images for the blurring caused by variations in the depth-of-interaction in position-sensitive gamma ray detectors. In the case of a fine-cut 50×50×30 mm BGO block detector, the method is shown to improve the detector resolution by about 25%, measured in the geometry corresponding to detection at the edge of the field-of-view. Strengths and weaknesses of the method are discussed and its potential usefulness for improving the images of future PET cameras is assessed.

Keywords: PET Detectors, Depth-of-Interaction, Image Blurring Correction

(submitted to IEEE Transactions on Medical Imaging)

I. Introduction

Depth-of-interaction variation in PET detectors is a long-standing problem[1] and various solutions have been proposed[2-4]. Present commercial PET cameras have not employed the proposed solutions, presumably because to do so would require more complicated and therefore more expensive detectors than the detectors commonly employed[5]. In a typical whole body PET camera[6], depth-of-interaction variations account for a 50% degradation in the radial component of image resolution at the edge of the 40 cm diameter field-of-view(FOV). As a percentage effect, this loss in resolution will be worse in future commercial cameras which will have increasingly better spatial resolution. For example, in the very-high-resolution Donner-600 camera, the loss in radial resolution is 60% only 8 cm from the centre of the FOV[2].

This article proposes correcting for depth-of-interaction variation, using a new method which will be shown to have certain advantages over the previous methods[2-4]. The new method has been tested in a particular block BGO detector, which evolved[7] from the detectors commonly used in Siemens-CTI PET cameras[5]. New detectors with 144 and 256 small crystals were made at CTI by cutting BGO blocks at finer intervals than is normally used. Comparisons were made with a standard CTI, 64-crystal block detector, which demonstrated the new detectors' substantially improved resolution and sampling capabilities. Because the finer-cut blocks proved difficult to calibrate using the normal 511 keV flood source, a new calibration procedure was developed using 4.44 MeV gamma rays[7].

II. The New Method Applied to a 256-crystal Block Detector

Figure 1 shows 511 keV pulse-height spectra, obtained by summing analog-to-digital converter (ADC) channels from all four PMT's attached to the back of the 256-crystal block. Figure 1a and 1b show normal flood spectra from two of the 256 crystals, selected as typical. The photopeaks show a bump or shoulder (depending on the crystal's position in the block) on the high energy side which is not present in the pulse-height spectra from the standard 64-crystal blocks [5]. To see if this new feature is a depth-of-interaction effect, the same block was exposed to a side-incident fan beam (formed as described in the next section) collimated to interact at one particular depth in the block. Figure 1c and 1d were acquired with gamma rays collimated to interact near (i.e. 4 mm from) the front face of the block. Figure 1e and 1f were acquired with gammas collimated to interact deep in the block, far (i.e. 23 mm) from the front face of the block. Many other depths were also tested to confirm the general trend shown in Fig. 1c-f. At each depth the photopeak is approximately Gaussian, but the maximum channel of the Gaussian shifts with depth in a predictable way. The further away from the front face the point of initial gamma interaction the larger is the most probable pulse-height channel of the photopeak. This one-to-one relationship between photopeak position and depth-of-interaction can be used to estimate the unknown depth-of-interaction in the normal PET geometry.

To make a substantial improvement in PET image blurring, the error in this depth-of-interaction estimate must be substantially smaller than the normal variation of the depth-of-interaction in the scintillator block. The essential requirement, which is met by the energy spectra of Fig. 1, is that the width of the peaks (Fig. 1c-f) must be substantially less than the shift in the central positions of the peaks between the

front (Fig. c-d) and back (Fig. e-f) of the block. This condition was not met in the conventional 64-crystal block or in the new 144-crystal block.

To test the method, a fan-collimated beam was used in two different geometries which duplicate the typical geometries of a PET camera imaging activity at the centre and at the edge of the FOV. The fan beam was formed by placing a Ge-68 point source at a distance of 12 cm from a pair of 5 cm thick Pb bricks which had a 1 mm wide vertical slit between their edges. When the plane of the fan was perpendicular to the face of the detector, the image of the beam was narrow, as it would be in imaging such activity at the centre of a PET camera. When the plane of the fan was inclined at a 25° angle to the normal, the image was broadened and shifted due to the depth-of-interaction variation in the detector. The desired objective of the correction method, which is the subject of this article, was to correct the broadened image to make it look more like the narrow image. The angle selected for this test was chosen to be 25° because this is a worst case maximum of the angles encountered in imaging activity distributions near the edges of the FOV of typical whole body PET cameras.

Figure 2 is a top-view schematic drawing of the beam impinging on one horizontal row of the 256-crystal block detector. A typical gamma ray is shown interacting in the small crystal number "10", which would be the one identified by the decoding system. The identified crystal numbers for other gamma rays entering the block along the same line will vary randomly among the crystals intersected by the line, namely crystal numbers 7, 8, 9, 10, and 11. Only by measuring the depth-of-interaction, Z, can the crystal number be corrected (by $\Delta X = Z \times \sin 25°$) to what it would have been if the gamma had interacted at the front face of the block.

In order to correct the crystal number, the depth Z must be measured in units of the crystal's spacing, 3.125 mm. Because each crystal has a different positron relative to the PMT's, and therefore different light collection efficiency, a look-up-table was required to relate the measured photopeak ADC number to depth-of-interaction in mm. This look-up-table was a list of "most probable depths" as a two-dimensional function of crystal number and summed ADC pulse-height. It was formed from depth calibration measurements, which were separately acquired prior to analyzing the fan-beam gamma event records.

The table was obtained by analyzing the individual crystals' pulse- height spectra, such as those shown in Fig. 1c-f. Each spectrum contains a single photopeak and a low level Compton tail below the photopeak. The peak channel of the photopeak in each spectrum is the most probable pulse-height at the fixed depth of the calibration setup. A table of depths as a function of most-probable pulse-height was formed by linear interpolation between the two measured photopeak pulse-heights (e.g. Fig. 1c-f) in each crystal.

It was discovered that the optimum scale factor (which was used for converting Z to ΔX), was about 30% smaller than the expected $\sin 25°$. This is believed to be due to an observed non-linearity in the relationship between depth-of-interaction and pulse-height. (It was observed that the pulse-height changes more slowly as a function of depth near the front face than it does deeper in the block). The linear interpolation mentioned above was an approximation, adopted for simplicity.

The upper and lower pulse-height thresholds were carefully set in each crystal so as to maintain uniform efficiency across the block. The lower-level pulse-height threshold was set in each crystal to be 0.92 of the photopeak pulse-height measured using

the shallow depth (4 mm) calibration setup. The upper-level pulse-height threshold was set to 1.10 of the photopeak pulse-height measured using the deep depth (23 mm) calibration setup. This choice of thresholds produced a measured block average efficiency of 0.74 relative to the efficiency of the block with "wide-open" (i.e. 250 keV lower- and 750 keV upper-level) thresholds.

To account for efficiency differences and any possible crystal identification errors in the calibration setup map, a flood source of 511 keV gammas was used for normalizing the two fan-beam images. A point source of 511 keV gamma rays was positioned at a distance from the 256-crystal block so that a flood of gamma rays impinged on the block in a direction approximately normal to the front face. Two 16 × 16 arrays of counts were acquired from this flood source with the pulse-height thresholds just described, both with and without employing the depth correction method. The flood source counts in these 16 × 16 arrays were divided crystal-by-crystal into the corresponding 16 × 16 arrays of counts from the fan-beam phantoms to produce the final normalized projections.

III. Results and Discussion

Figure 3 shows one-crystal-wide horizontal sections of the phantom images at three different (typical) positions on the face of the 256-crystal block. The normal-angle sections (Fig. 3a-c) are broadened and shifted by depth-of-interaction blurring (Fig. 3d-f), which is substantially improved using the above-described correction method (Fig. 3g-i). The improvement between the uncorrected sections (Fig. 3d-f) and the corrected sections (Fig. 3g-i) ranged from 17% to 30% over the face of the detector, averaging a 25% improvement in the FWHM.

It is believed that the variation in pulse-heights between shallow and deep-interacting gamma rays is due to the variation in the number of scintillation photons absorbed on the side walls of the crystals. The amount of variation could therefore be adjusted to be a larger fraction of the original scintillation light by reducing the reflectivity of the sides of the individual crystals making up the block. Although this would improve the depth-of-interaction resolution, such a "detuning" of the light collection would probably worsen the accuracy of the usual determination of the X- and Y-coordinates of the crystal of first-interaction. A range of trade-offs between XY-resolution and Z-resolution should be possible.

A fraction of events are under-corrected because the gamma energy was degraded by Compton outscattering from the block. This fraction can be roughly estimated as the fractional number of Compton-scattered events in Fig. 1a-b compared to photopeak events, 19% and 32%, respectively. The variation of this effect as a function of threshold was not measured, but it would certainly be increasingly important at lower thresholds. Gamma rays which have scattered in the object and therefore enter the block with degraded energy are similarly under-corrected. However, these gamma rays are already so disturbed in position that they form a smoothly varying background which can therefore be eliminated from the image using one of the existing object-scatter correction techniques [8]. Such low frequency image correction [8] would probably best be done after the depth-of-interaction correction, which effects more the high-frequency components of the image.

IV. Conclusions

I have presented a new method of correcting for depth-of-interaction blurring in block BGO detectors. The method has the advantage over other methods[2-4] in that it is simple to apply and does not require extra photodetectors. The method was verified to improve the measured FWHM line spread by about 25% in a simple test case in which a beam of 511 keV gamma rays impinged at 25° to the normal into a 30 mm thick block of BGO.

The method should theoretically work even better for block detectors incorporating brighter scintillators, denser scintillators, or more efficient photodetectors than my 256-crystal BGO block detector. The method seems to have the potential for substantially reducing the principal source of resolution loss at the edges of the field of view of typical commercial PET cameras.

V. Acknowledgement

The continuing support and encouragement of Dr. Ronald Nutt of CTI is gratefully acknowledged. Thanks go to Mike Stazyk for suggesting several useful improvements in the manuscript.

VI. References

[1] J.G. Rogers, "Testing an improved scintillation camera for PET and SPECT", *IEEE Trans. Nucl. Sci.*, vol. NS-33, pp. 519-522 (1986).

[2] S.E. Derenzo, W.W. Moses, H.G. Jackson, B.T. Turko, J.L. Cahoon, A.B. Geyer, and T. Vuletich, "Initial characterization of a position-sensitive photodiode/BGO detector for PET", *IEEE Trans. Nucl. Sci.*, vol. NS-36, pp. 1084-1089 (1989).

[3] T. Yamashita, M. Watanabe, K. Shimizu, and H. Uchida, "High resolution block detectors for PET", *IEEE Trans. Nucl. Sci.*, vol. NS-37, pp. 589-593 (1990).

[4] P. Bartzakos and C.J. Thompson "A depth-encoded PET detector", *Trans. Nucl. Sci.*, vol. NS-38, pp. 732-738 (1991).

[5] J.G. Rogers, A.J. Taylor, M.F. Rahimi, R. Nutt, M. Andreaco, and C.W. Williams, "An improved multicrystal BGO detector for PET", *IEEE Trans. Nucl. Sci.*, vol. NS-39, pp. 1063-1068 (1992).

[6] T.J. Spinks, T. Jones, M.C. Gilardi, and J.D. Heather, "Physical performance of the latest generation of commercial positron scanner", *IEEE Trans. Nucl. Sci.*, vol. NS-35, pp. 721-725 (1988).

[7] J.G. Rogers, R. Nutt, M. Andreaco, and C.W. Williams, "Testing 144- and 256-crystal BGO block detectors for PET", presented November 6, 1993 at IEEE Nuclear Science Symposium and Medical Imaging Conference, San Francisco.

[8] J.S. Barney, J.G. Rogers, R. Harrop, and H. Hoverath, "Object shape dependent scatter simulations for PET", *IEEE Trans. Nucl. Sci.*, vol. NS-38, pp. 719-725 (1991).

Figure Captions

1. 511 keV gamma ray pulse-height spectra in individual crystals, counts as a function of channel, (a) flood source in central crystal; (b) flood source in edge crystal; (c) shallow source in central crystal; (d) shallow source in edge crystal; (e) deep source in central crystal; and (f) deep source in edge crystal.
2. Top view of inclined-beam and block detector geometry showing the mechanism of depth-of-interaction correction.
3. One-crystal-wide horizontal sections across the 256-crystal PET detector. (a) normal beam, central crystal; (b) normal beam, half-way-out crystal; (c) normal beam, edge crystal; (d-f) 25° inclined beam, same three sections; (g-i) 25° inclined beam with new correction method applied, same three sections.

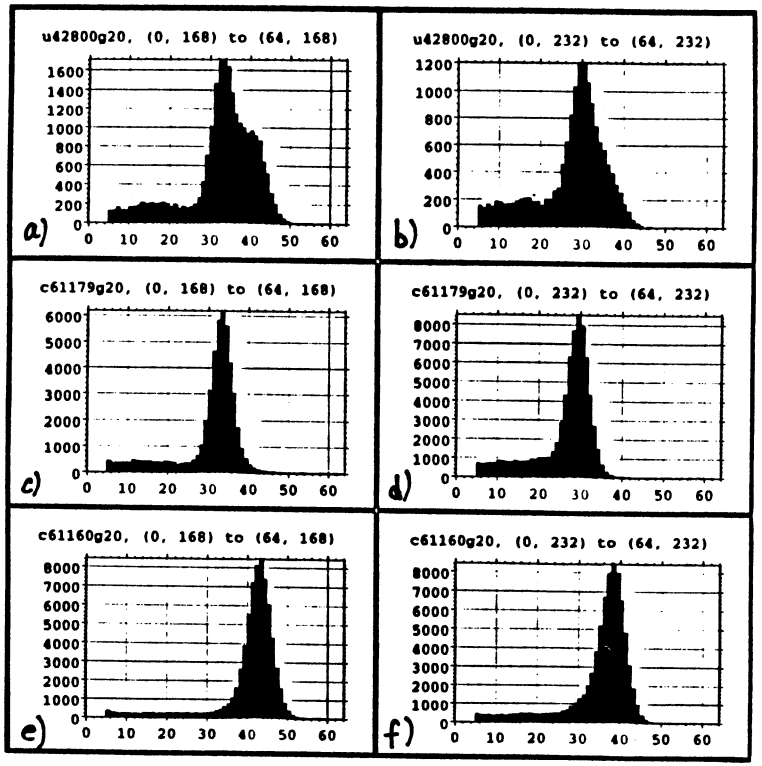

Fig. 1

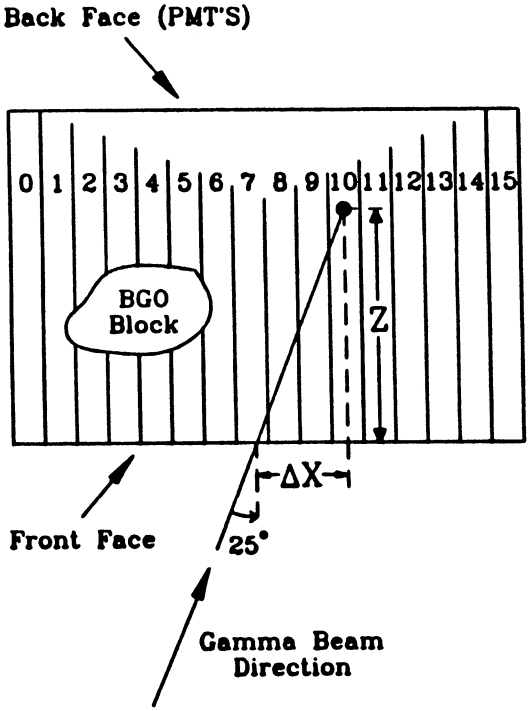
Back Face (PMT'S)
0 1 2 3 4 5 6 7 8 9 10 11 12 13 14 15
BGO Block
Z
ΔX
Front Face
25°
Gamma Beam Direction

Fig. 2

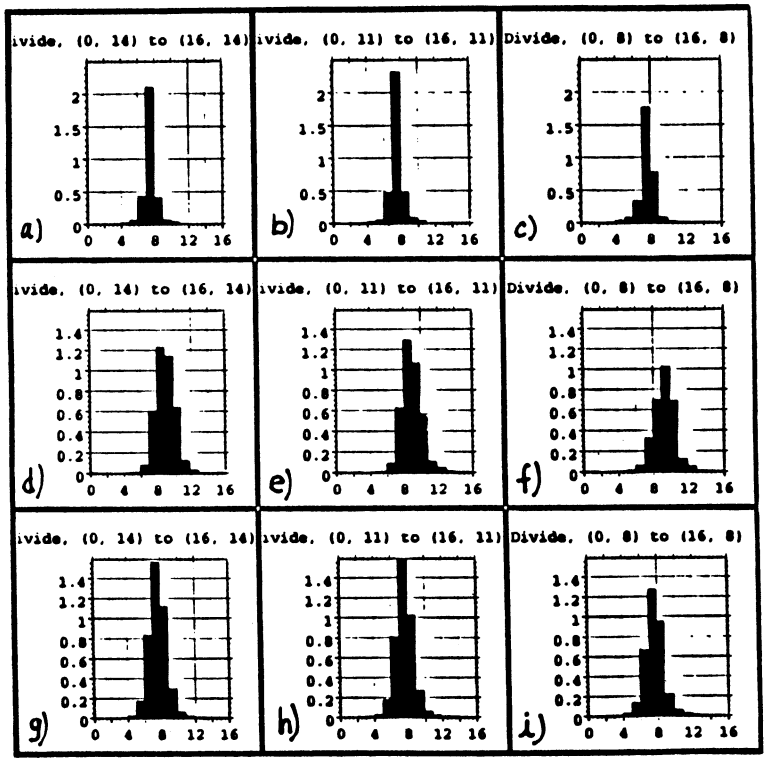
Divide, (0, 14) to (16, 14)
Divide, (0, 11) to (16, 11)
Divide, (0, 8) to (16, 8)
a)
b)
c)
d)
e)
f)
g)
h)
i)

Fig. 3